ARTICLE

Recent Implementations in LASP 3.0: Global Neural Network Potential with Multiple Elements and Better Long-Range Description[†]

Pei-lin Kang, Cheng Shang*, Zhi-pan Liu*

Collaborative Innovation Center of Chemistry for Energy Material, Shanghai Key Laboratory of Molecular Catalysis and Innovative Materials, Key Laboratory of Computational Physical Science (Ministry of Education), Department of Chemistry, Fudan University, Shanghai 200433, China
Shanghai Qi Zhi Institute, Shanghai 200030, China

(Dated: Received on August 24, 2021; Accepted on September 8, 2021)

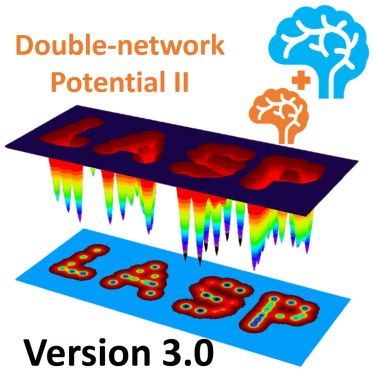

LASP (large-scale atomistic simulation with neural network potential) software developed by our group since 2018 is a powerful platform (www.lasphub.com) for performing atomic simulation of complex materials. The software integrates the neural network (NN) potential technique with the global potential energy surface exploration method, and thus can be utilized widely for structure prediction and reaction mechanism exploration. Here we introduce our recent update on the LASP program version 3.0, focusing on the new functionalities including the advanced neural network training based on the multi-network framework, the newly-introduced S^7 and S^8 power type structure descriptor (PTSD). These new functionalities are designed to further improve the accuracy of potentials and accelerate the neural network training for multiple-element systems. Taking Cu−C−H−O neural network potential and a heterogeneous catalytic model as the example, we show that these new functionalities can accelerate the training of multi-element neural network potential by using the existing single-network potential as the input. The obtained double-network potential CuCHO is robust in simulation and the introduction of S^7 and S^8 PTSDs can reduce the root-mean-square errors of energy by a factor of two.

Key words: Large-scale atomistic simulation with neural network potential, Machine learning, Neural network, Structure descriptor, Simulation software

I. INTRODUCTION

Recent years have seen rapid development of machine learning (ML) potentials and their implementation in various software packages, such as GAP [1], DeepMD [2], SchNet [3], ANI-1 [4], AMP [5], QML models [6], LASP [7] *etc.* By using different structure descriptors, those ML potentials convert the coordinate information of atomic models into the input of ML potential, and produce total energy and atomic forces as the output. This replaces the difficult procedure of solving the Schrödinger equation in performing atomic simulation. LASP software (large-scale atomistic simulation with neural network Potential) developed by us in 2018 [7], is the first practice to combine the global potential energy surface (PES) exploration methods with the high dimensional neural network (NN) technique to achieve the global PES exploration with global neural network potentials (G-NN). Due to the global representativity

[†]Part of special topic of "Young Scientist Forum on Chemical Physics (Theory and Calculation Workshop 2020)".

*Authors to whom correspondence should be addressed. E-mail: cshang@fudan.edu.cn, zpliu@fudan.edu.cn

DOI:10.1063/1674-0068/cjcp2108145

of the dataset from global optimization, LASP software is particularly useful for predicting the unknown structures and reactions in complex systems. This has indeed become one of the major driving forces to develop ML potential techniques, as more and more applications emerge from the fields of structure prediction of new materials [8, 9] and heterogeneous catalysis mechanism exploration [10, 11]. To date, one of the outstanding challenges in the ML potential technique is to incorporate more elements and thus more datasets in potential training for complex and diverse chemical systems. Herein we describe the recent progress on LASP software development, which shows a promising way to fast train NN potentials for multi-element systems with high accuracy.

Following the Behler-Parrinello proposal that the total energy of a system can be considered as the sum of individual atoms [12], the current ML potentials are generally atom-wise, *i.e.*, each atomic energy is fitted individually by a ML model such as NN. In this scheme, the incorporation of multiple elements of the system should be implemented in the structure descriptors for each atom. A simple way is to not discriminating explicitly elements in the ML model and also in the atomic structure descriptors [12]. This can significantly reduce the cost of ML potential with all elements sharing a single ML model and with much fewer structure descriptors for each atom, but is apparently at the expense of fine structure discrimination of atomic chemical environment and thus the accuracy of ML potential. This simple way is adopted in early ML potentials and gradually abandoned in recent practices. It is also likely to introduce different parameters for different elements [13] in computing atomic structure descriptors, which however will not improve significantly the accuracy. On the other hand, the more advanced way is to discriminate elements by using different atomic structure descriptors, as implemented in LASP software [8, 14]. This approach assigns different ML (*e.g.* NN) models for different elements, and the atomic structure descriptors can naturally distinguish different elements. As a result, the accuracy of the multi-element potential is in principle as good as that of the single-element potential. Unfortunately, the explicit element-discrimination will eventually lead to the explosion of the number of structure descriptors for each ML model with too many ML parameters to determine, and thus the training and the application of ML potentials becomes computationally too demanding.

Another key difficulty in ML potentials is to describe the long-range interaction accurately, which is generally small in energy but can be of great significance in chemical reactions. The current atomic structure descriptor generally involves the summation of all neighbor contributions, from the local range to the middle and long-range [14, 15]. The typical cutoff for atomic structure descriptors in practice is often 7−8 Å. While this approach maintains the translation-rotation-permutation invariance, it inevitably sacrifices the accuracy in describing the long-range interaction since the contributions from long-range neighbors are always mixed with those from the short-range neighbors. A possible solution is to explicitly introduce the long-range interactions, such as electrostatic term, in ML potentials, as demonstrated in recent literatures [16, 17]. However, the accurate electrostatic interaction requires accurate data on the atomic charge that are generally difficult to obtain from electronic structure calculations.

Here we report our recent efforts in developing LASP software, focusing on constructing the G-NN potential for multi-element systems and for those with important middle-long range interactions. This work is organized as follows. In section II, we introduce briefly the current functions in LASP version 3.0, focusing on the recently implemented training module. In section III, we introduce the new structure descriptors designed for better long-range interaction learning and the double-network architecture designed for fast training of multi-element potentials. In section IV, the new descriptors and NN architecture are benchmarked by a heterogeneous catalytic system, showing good training efficiency, stability, and accuracy.

II. A BRIEF INTRODUCTION OF LASP VERSION 3.0

The LASP software version 1.0 was first released in 2018 [18]. Its main functions, as schematically illustrated in FIG. 1, include potential energy calculation, potential energy surface (PES) exploration, MD simulation, and NN potential training. In the potential energy calculation section, LASP provides not only G-NN potential, but also standard data-exchange interfaces to connect with common PES evaluation packages, which allows for the PES data generation using quantum mechanics calculation and empirical force fields. The PES exploration modules include global structure search and pathway sampling based on Stochastic surface walking

DOI:10.1063/1674-0068/cjcp2108145

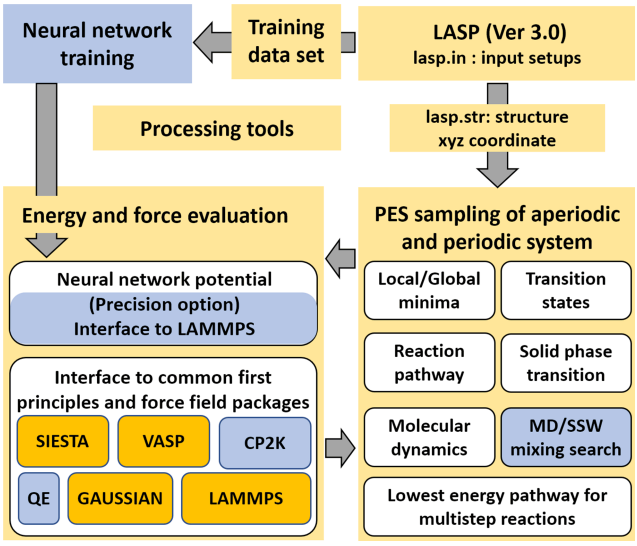

FIG. 1 Architecture and the modular map of LASP version 3.0. The newly added functions are highlighted in blue.

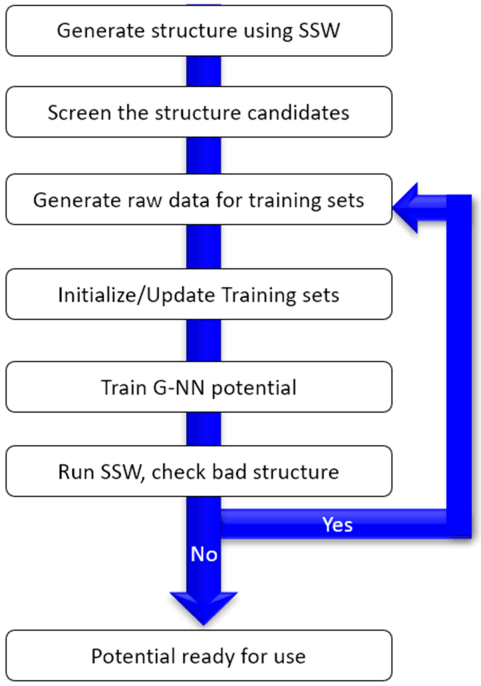

FIG. 2 A schematic flowchart on generating G-NN potential using LASP.

(SSW) method [19, 20], transition state location based on Constrained Broyden Dimer (CBD) method [21] and Double-Ended Surface Walking (DESW) method [22]. All those methods can be performed for both fixed and variable cell systems. MD simulation modules are also included in LASP, including the micro-canonical, canonical, isothermal-isobaric ensembles (NVE, NVT, NPT)[23] and enhanced sampling with specifiable restraints. The Verlet algorithm is utilized to integrate the equation of motion. The thermostat and barostat utilized in NVT and NPT adopt Nose-Hoover [23, 24] and Parrinello-Rahman methods [25], respectively.

In version 3.0, we have implemented some new functions, including: (i) training module for G-NN potential generation, (ii) interface of NN potentials to LAMMPS program, (iii) interface of CP2K [26] and Quantum Espresso [27] to LASP, (iv) combined MD SSW simulation for PES exploration. Based on the training module, we have accomplished a self-consistent using procedure of LASP. A flowchart is shown in FIG. 2 and described as follows:

(1) Generate structure candidate for training set: Performing SSW simulation using first principle computations at a low-precision level to rapidly generate the first batch of structure candidates. The output of structures is controlled by simple keywords in the input files. The previous study has demonstrated that SSW method can explore more extensive on PES than traditional MD simulation and sample more chemical environments.

(2) Screening the structure candidates: Removing duplicated structures and those with large forces (*e.g.* maximum components of atomic forces >10 eV/Å), which is often irrelevant to the chemical process, however causing great trouble to the training.

(3) Generate raw data for training sets: Computing all structures using first principle computation at relatively high precision. The structures, energies, forces and stresses are printed in LASP standard format.

(4) Initialize/update training sets: Collecting all the raw data and transform them into standard training input files (TrainStr.txt and TrainFor.txt), which is achieved using a python script provided in LASP package.

(5) Train G-NN potential: Performing G-NN potential training using LASP with simple keywords in the input files. A set of structure descriptors and network architecture are required as input to initialize the network architecture, which can either be provided by user, or be generated by LASP automatically with default settings. The training of NN parameters is achieved using the 1-BFGS method, where the number of total training epoch is set as the stop criterion.

(6) Run SSW and refine the training sets: Performing SSW or MD simulation using the trained potential. Two kinds of "bad" structures will be printed out au-

DOI:10.1063/1674-0068/cjcp2108145

tomatically, namely structures with PTSDs beyond the range of potential and structures with validated energies much lower than the expected values. As an option, other structures of the trajectory are also printed by predefined frequency.

(7) Repeat (3)−(6) until no "bad" structures are present. At the moment, the learning cost for a three-element system (*e.g.* Ti, O, H system) G-NN potential is, typically, one to two weeks' computation of ∼1000 CPU cores.

III. NEW DESCRIPTORS AND THE DOUBLE-NETWORK FRAMEWORK

The G-NN potential in LASP follows the high-dimensional neural network architecture proposed by Behler and Parrinello in 2007 [12], where the potential energy of the system is decomposed into the sum of individual atom energies. The feed forward NN is utilized to predict the atomic energy, where the input nodes of the NN are a set of coordinate-based structural descriptors to maximally distinguish structures on PES, called as the power type structural descriptors (PTSDs) [14], which consists of up to four body terms as shown in Eq.(1−8). The PTSDs take the translation- and rotation-invariant geometrical parameters, including the atom pair distance, the angle among three atoms and the torsion angle among four atoms as the variables, combining them using the power, cosine and spherical functions to construct the n-body (two-, three- and four-body) structure descriptors.

$$f_c(R_{ij}) = \begin{cases} 0.5 \times \tanh^3\left[1 - \dfrac{r_{ij}}{r_c}\right] & \text{for } r_{ij} > r_c, \\ 0 & \text{for } r_{ij} \leq \mathrm{r}_c \end{cases} \quad (1)$$

$$R^n(r_{ij}) = r_{ij}^n \cdot f_c(r_{ij}) \quad (2)$$

$$S_i^1 = \sum_{j\neq i} R^n(r_{ij}) \quad (3)$$

$$S_i^2 = \left[\sum_{m=-L}^{L}\left|\sum_{j\neq i} R^n(r_{ij})Y_{Lm}(r_{ij})\right|^2\right]^{1/2} \quad (4)$$

$$S_i^3 = 2^{1-\zeta}\sum_{j,k\neq i}(1+\lambda\cos\theta_{ijk})^{\zeta}\cdot R^n(r_{ij})\cdot R^m(r_{ik})\cdot R^p(r_{jk}) \quad (5)$$

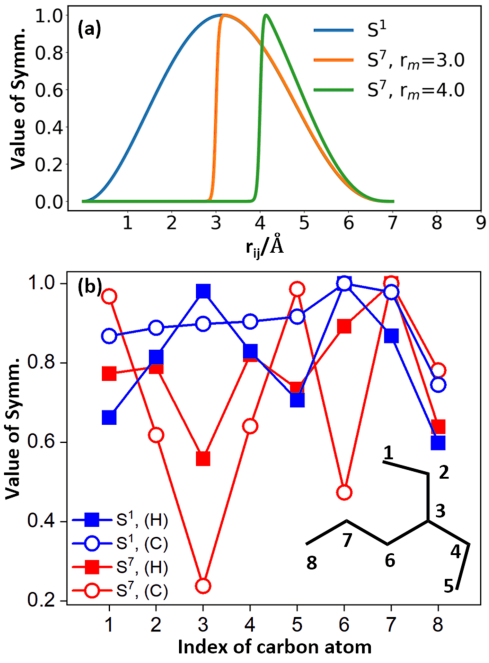

FIG. 3 (a) Values of S^1 (blue curve) and S^7 (orange and green curves) function with respect to the distance. The cutoff r_c=7.0 and n=2 in all three cases. The parameter α in S^7 equals to 16. (b) Values of S^1 (blue) and S^7 (red) of carbon atoms in 3-ethylhexane molecule by considering carbon-hydrogen (solid square) and carbon-carbon (hollow circle) as atom pairs, respectively. The cutoff r_c=7.0 and n=2 in all three cases. The parameters α and r_m in S^7 equals 16 and 3.0, respectively. The molecule with the labeled index of carbon is inserted.

$$S_i^4 = 2^{1-\zeta}\sum_{j,k\neq i}(1+\lambda\cos\theta_{ijk})^{\zeta}\cdot R^n(r_{ij})\cdot R^m(r_{ik}) \quad (6)$$

$$S_i^5 = \left[\sum_{m=-L}^{L}\left|\sum_{j,k\neq i} R^n(r_{ij})\cdot R^m(r_{ik})\cdot R^p(r_{jk}) \cdot\Big(Y_{Lm}(r_{ij}) + Y_{Lm}(r_{ik})\Big)\right|^2\right]^{1/2} \quad (7)$$

$$S_i^6 = 2^{1-\zeta}\sum_{j,k,l\neq i}\cdot(1+\lambda\cos\delta_{ijkl})^{\zeta}R^n(r_{ij})R^m(r_{ik})R^p(r_{il}) \quad (8)$$

$$S_i^7 = \sum_{j\neq i} R^n(r_{ij}) \times \{1 + \tanh[\alpha\cdot(r_{ij} - r_m)]\} \quad (9)$$

$$S_i^8 = \left\{\sum_{m=-L}^{L}\left|\sum_{j\neq i} R^n(r_{ij})Y_{Lm}(r_{ij}) \cdot\Big\{1 + \tanh\Big[\alpha\cdot\Big(r_{ij} - r_m\Big)\Big]\Big\}\right|^2\right\}^{1/2} \quad (10)$$

In LASP version 3.0, we have designed two new de-

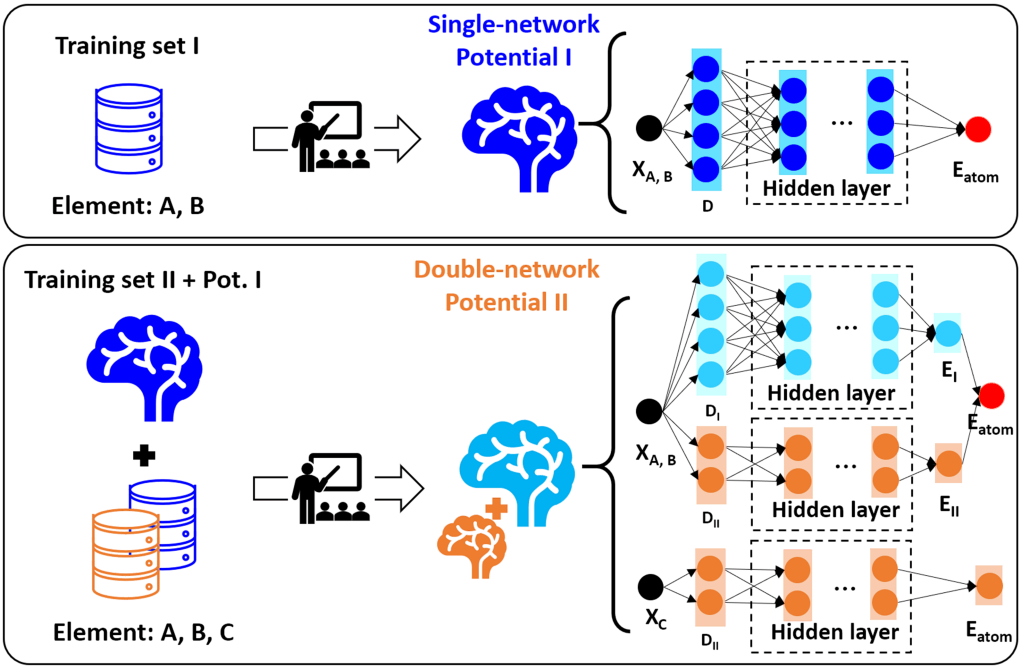

FIG. 4 A schematic illustration of the double-network framework. X represents the Cartesian coordinates of each atom. $E_{\rm atom}$ represents the atomic energy of each atom. D represents the PTSD used in NN.

scriptors, namely S^7 and S^8, aiming at enhancing the description of the chemical environment contributed by atoms not binding to the central atom. Similar ideas have also been implemented in some piecewise descriptors by Jiang and co-workers to save computational costs [28]. The mathematic forms of two descriptors are as Eq.(9) and Eq.(10), which is S^1 and S^2 multiplied by a hyperbolic tangent type function to each pair contribution. FIG. 3(a) shows the comparison between S^1 and S^7 with different parameters, where the newly designed S^7 only responds to neighboring atoms away from the central atoms by a distance beyond $r_{\rm m}$. For a real molecule, *i.e.* 3-ethylhexane, the S^1 and S^7 exhibit remarkable differences in carbon, especially when computing C−H atom pairs, where carbon atoms have similar S^1 values but rather diverse S^7 values. In practice, we always pick $r_{\rm m}$ larger than 2.0 Å, which basically eliminates all the first neighboring atoms that having strong interaction with the central atom. It is worth mentioning that the curve looks steep when approaching $r_{\rm m}$ from zero in FIG. 3(a), mainly because we choose a large value of α, which is 16, to show the feature of the S^7 descriptor. In practice, the values of α are randomly selected in the range of 2−16, which is also the range of n that is used in all descriptors, where a smaller value makes the curve gentler.

To improve the training efficiency of multi-element potentials, we have designed a double-network framework in the LASP program version 3.0. A schematic illustration is shown in FIG. 4, where a three-element potential, *i.e.* A-B-C potential is the target to be trained. To initiate, a single-network potential I has already been trained for most of the elements, such as A and B in the example. The A-B potential together with another newly initiated full-element potential are then used as input to learn an extended training set II. The obtained double-network potential II is composed of two sub-potentials, where the full-element sub-potential (sub-pot. II) generally has a smaller network than the sub-potential I. The atomic energies of elements A and B atoms are evaluated by both sub-potentials, being equal to the sum of the output of both sub-potentials. The atomic energies of element C atoms are evaluated by sub-pot. II only.

IV. BENCHMARK OF THE DOUBLE-NETWORK POTENTIAL

A. Training efficiency of a Cu-C-H-O double-network potential

We firstly exam the performance of the double-network architecture in training a four element Cu-C-H-O potentials. A previously trained C-H-O potential

DOI:10.1063/1674-0068/cjcp2108145

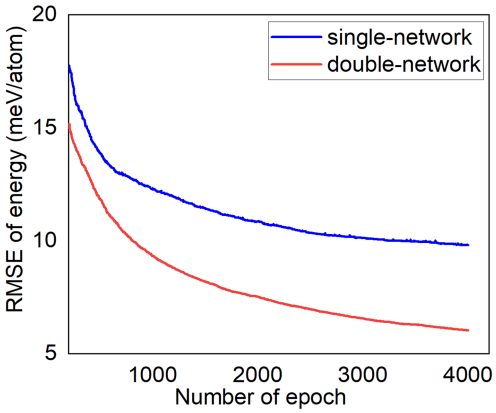

FIG. 5 The training efficiency of the double-network and the single-network architectures on training the Cu-C-H-O NN potential.

is used as the network set I, where a five-layer (258-97-70-40-1) NN architecture is used for C, H, and O elements, corresponding to 97683 parameters in total. This C-H-O potential is trained on a data set containing 10255 structures, where the root-mean-square errors (RMSE) for the energy and the force of the C-H-O potential are 6.845 meV/atom and 0.202 eV/Å, respectively. The second set of Network contains all four elements with a four-layer architecture (274-50-50-1), corresponding to 65404 parameters, which are randomly initiated at the beginning. A training data set containing 91405 structures is used for test. FIG. 5 shows the training efficiency of the double-network framework (red curve). The training RMSE of energy reduces from 2105.3 meV/atom (not shown in FIG. 5) at the beginning to 6.0 meV/atom after 4000 epochs, which is accurate enough for MD and SSW simulations. For comparison, we have also examined the performance of the network set II along on training the same data set, which is shown as the blue curve in FIG. 5. The training RMSE of energy then only reduces to 9.8 meV/atom at 4000 epochs and to 9.5 meV/atom by extending to 5000 epochs.

B. Benchmark of the robustness of Cu-C-H-O potential

Using the trained Cu-C-H-O double-network potential, we then perform a 2 ns molecular dynamics (MD) simulation at 500 K on a heterogeneous catalytic system, namely, glycerol conversion on metal surfaces, which has attracted much attention in recent years for its potential application as biomass energy [29–31]. As shown in FIG. 6(a−c), a four-layer Cu(111) (4×4) slab model is built with the bottom three layers fixed. A ketone molecule with four dissociated H atoms are all adsorbed on the surface to simulate a possible intermediate of the glycerol decomposition, where four water molecules are also put in the gas phase. A biased potential is added at 10 Å above the slab surface to prevent molecules from flying away. From the MD trajectories, we found massive adsorption/desorption processes of water and ketone molecules, as well as hydrogen atoms diffusion on the surface. No reaction is observed within 2 ns. The simulation trajectory is shown in FIG. 6(d), where the variation of the conserved total energy is within 0.05 eV from average in the 2 ns simulation, indicating the robustness of the potential.

C. Benchmark of accuracy Improvement of double network architecture and S^7 and S^8 PTSDs

20 configurations are picked from the MD trajectory by every 0.1 ns to exam the accuracy of the current Cu-C-H-O potential. The benchmarking data are computed using the same setup as the training data set. Here we use a plane wave DFT code, VASP, [32, 33] where electron-ion interaction is represented by the projector augmented wave (PAW) pseudopotential [32]. The kinetic energy cutoff utilized is 450 eV. The first Brillouin zone k-point sampling utilizes the Monkhorst-Pack scheme with an automated mesh determined by 25 times the reciprocal lattice vectors. The results are shown in FIG. 7 (blue triangle), where the DFT energy of the 0.1 ns configuration is set to be zero. The maximum error corresponding to 3.3 meV/atom, which is less than the training RMSE. The average error of 20 points is 1.3 meV/atom.

Using the same model, we then investigated the effect of S^7 and S^8 PTSDs on improving the accuracy of the potential. Two extra Cu-C-H-O single-network potentials are fitted with the S^7 and S^8 PTSD included or not. The structure of the network is 410-80-80-48-1 for $S^{7,8}$-included potential (pot 1), corresponding to 173188 parameters; and 352-80-80-48-1 for $S^{7,8}$-absence potential (pot 2), corresponding to 154628 parameters. The training RMSE of energy is 8.7 and 9.4 for pot 1 and pot 2, respectively. Using both potentials we have benchmarked the same data set and plotted in FIG. 7 (red circle and black square). The maximum and average errors are 5.7 and 2.7 meV/atom for pot 1 and 10.5 and 5.9 meV/atom for pot 2, indicating that the S^7 and S^8 PTSD can improve the efficiency by a factor

DOI:10.1063/1674-0068/cjcp2108145

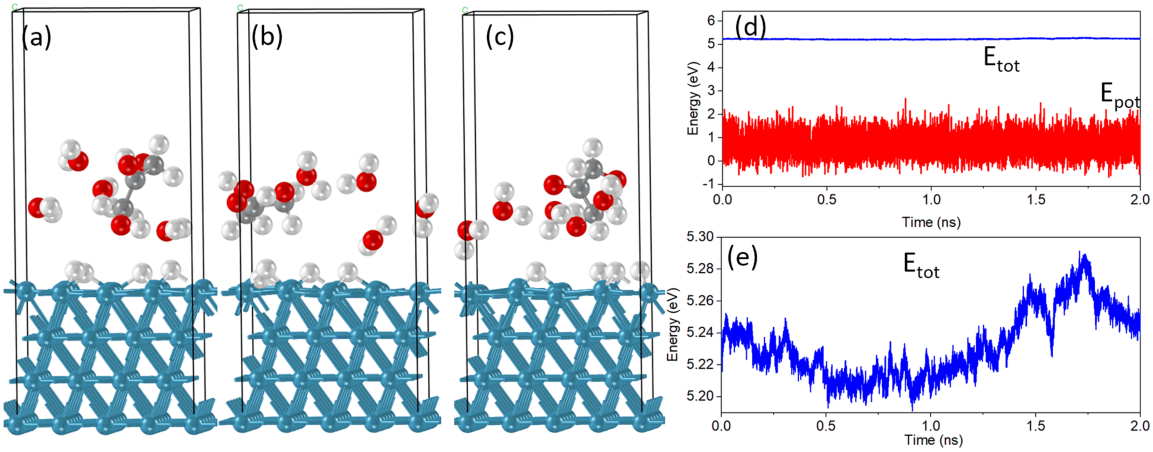

FIG. 6 Theoretical model (a) and MD trajectory (b) of glycerol conversion intermediate state on Cu(111) slab. (a−c): The configuration at 1 ps, 1 ns and 2 ns, respectively; white: hydrogen, red: oxygen, grey: carbon, blue: copper. (d) the potential energy (red) and the conserved total energy (blue), which is expanded in (e). The step size is 0.5 fs.

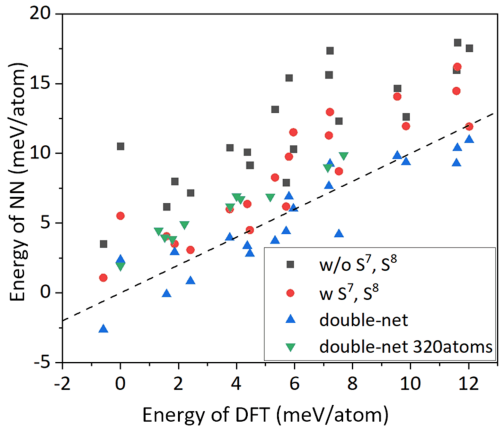

FIG. 7 Benchmark of different Cu-C-H-O NN potentials on the accuracy of energy evaluation. 20 points are obtained along the MD trajectories of a slab model containing 92 atoms by every 0.1 ns. The blue triangle, red circle and black square represent the data computed by the double-network potential, single-network potential with $S^{7,8}$ PTSD and single-network potential without $S^{7,8}$ PTSD, respectively. An expanded slab model containing 320 atoms is also used to benchmark the extensiveness of the double-network potential as represented by the green triangle. The DFT energy of the 0.1 ns configuration is set to be zero.

of two for such a heterogeneous catalytic system. One possible reason for this improvement is that the S^7 and S^8 PTSD have enhanced the learning ability of the potential for weak interactions such as between different molecules and between molecules and the surface. We have also performed a benchmark on a $(4\sqrt{3}\times8)$ slab model with four ketone molecules (320 atoms in total). Ten configurations are obtained along a 1 ps short MD trajectory by every 0.1 ps, and the maximum error is 3.16 meV/atom, indicating good extensiveness of the current potential.

V. CONCLUSION

This work summarizes the recent progress on LASP software development. We show that the multi-network framework is particularly useful for multi-element potential training, which can reuse the previous dataset and shorten the NN training time. This allows the NN potential to have a better transferability in real applications that contain multiple elements with multiple valences. By using a double-network Cu-C-H-O potential training as an example, we show that the new framework can speed up the training efficiency by 50% compared to the single-network training on the same dataset. The obtained double-network potential is robust and accurate in long-time MD simulation. We also show that the new-designed S^7 and S^8 PTSD can enhance the accuracy of NN potential for simulating heterogeneous catalytic systems, which should be due to the emphasis on the middle-long range interaction between floating molecules and surface atoms.

VI. ACKNOWLEDGMENTS

This work was supported by the National Key Research and Development Program of China (No.2018YFA0208600) and the National Natural Science Foundation of China (No.91945301, No.22033003, No.92061112, No.22122301, and No.91745201).

DOI:10.1063/1674-0068/cjcp2108145

[1] A. P. Bartók and G. Csányi, Int. J. Quantum Chem. **115**, 1051 (2015).
[2] H. Wang, L. Zhang, J. Han, and W. E, Comput. Phys. Commun. **228**, 178 (2018).
[3] K. T. Schütt, H. E.Sauceda, P. J. Kindermans, A. Tkatchenko, and K. R. Müller, J. Chem. Phys. **148**, 241722 (2018).
[4] J. S. Smith, O. Isayev, and A. E. Roitberg, Chem. Sci. **8**, 3192 (2017).
[5] A. Khorshidi and A. A. Peterson, Comput. Phys. Commun. **207**, 310 (2016).
[6] F. A. Faber, A. S. Christensen, B. Huang, and O. A. v. Lilienfeld, J. Chem. Phys. **148**, 241717 (2018).
[7] S. D. Huang, C. Shang, P. L. Kang, X. J. Zhang, and Z. P. Liu, WIREs Comput. Mol. Sci. **9**, e1415 (2019).
[8] S. D. Huang, C. Shang, X. J. Zhang, and Z. P. Liu, Chem. Sci. **8**, 6327 (2017).
[9] S. Ma, C. Shang, C. M. Wang, and Z. P. Liu, Chem. Sci. **11**, 10113 (2020).
[10] Y. Zhu, J. He, C. Shang, X. Miao, J. Huang, Z. Liu, H. Chen, and Y. Han, J. Am. Chem. Soc. **136**, 12746 (2014).
[11] X. T. Li, L. Chen, C. Shang, and Z. P. Liu, J. Am. Chem. Soc. **143**, 6281 (2021).
[12] J. Behler and M. Parrinello, Phys. Rev. Lett. **98**, 146401 (2007).
[13] Y. Zhang, C. Hu, and B. Jiang, J. Phys. Chem. Lett. **10**, 4962 (2019).
[14] S. D. Huang, C. Shang, P. L. Kang, and Z. P. Liu, Chem. Sci. **9**, 8644 (2018).
[15] C. Shang, S. D. Huang, and Z. P. Liu, J. Comput. Chem. **40**, 1091 (2019).
[16] X. Xie, K. A. Persson, and D. W. Small, J. Chem. Theory Comput. **16**, 4256 (2020).
[17] T. W. Ko, J. A. Finkler, and S. Goedecker, J. Behler, Acc. Chem. Res. **54**, 808 (2021).
[18] LASP Software.www.lasphub.com
[19] C. Shang, X. J. Zhang, Z. P. Liu, Phys. Chem. Chem. Phys. **16**, 17845 (2014).
[20] C. Shang and Z. P. Liu, J. Chem. Theory. Comput. **9**, 1838 (2013).
[21] C. Shang and Z. P. Liu, J. Chem. Theory Comput. **6**, 1136 (2010).
[22] X. J. Zhang, C. Shang, and Z. P. Liu, J. Chem. Theory. Comput. **9**, 5745 (2013).
[23] D. Frenkel and B. Smit, In *Understanding Molecular Simulation (Second Edition)*, D. Frenkel and B. Smit, Eds., San Diego: Academic Press, 139 (2002).
[24] N. Shuichi, Prog. Theor. Phys. Suppl. **103**, 1 (1991).
[25] M. Parrinello and A. Rahman, Phys. Rev. Lett. **45**, 1196 (1980).
[26] T. D. Kühne, M. Iannuzzi, M. D. Ben, V. V. Rybkin, P. Seewald, F. Stein, T. Laino, R. Z. Khaliullin, O. Schütt, F. Schiffmann, D. Golze, J. Wilhelm, S. Chulkov, M. H. Bani-Hashemian, V. Weber, U. Borštnik, M. Taillefumier, A. S. Jakobovits, A. Lazzaro, H. Pabst, T. Müller, R. Schade, M. Guidon, S. Andermatt, N. G. Holmberg, K. Schenter, A. Hehn, A. Bussy, F. Belleflamme, G. Tabacchi, A. Glöß, M. Lass, I. Bethune, C. J. Mundy, C. Plessl, M. Watkins, J. VandeVondele, M. Krack, and J. Hutter, J. Chem. Phys. **152**, 194103 (2020).
[27] P. Giannozzi, S. Baroni, N. Bonini, M. Calandra, R. Car, C. Cavazzoni, D. Ceresoli, G. L. Chiarotti, M. Cococcioni, I. Dabo, A. Dal Corso, S. de Gironcoli, S. Fabris, G. Fratesi, R. Gebauer, U. Gerstmann, C. Gougoussis, A. Kokalj, M. Lazzeri, L. Martin-Samos, N. Marzari, F. Mauri, R. Mazzarello, S. Paolini, A. Pasquarello, L. Paulatto, C. Sbraccia, S. Scandolo, G. Sclauzero, A. P. Seitsonen, A. Smogunov, P. Umari, and R. M. Wentzcovitch, J. Phys: Condens Matter. **21**, 395502 (2009).
[28] Y. Zhang, C. Hu, and B. Jiang, Phys. Chem. Chem. Phys. **23**, 1815 (2021).
[29] B. N. Zope, D. D. Hibbitts, M. Neurock, and R. J. Davis, Science **330**, 74 (2010).
[30] C. H. C. Zhou, J. N. Beltramini, Y. X. Fan, and G. Q. M. Lu, Chem. Soc. Rev. **37**, 527 (2008).
[31] J. ten Dam and U. Hanefeld, Chemsuschem **4**, 1017 (2011).
[32] G. Kresse and D. Joubert, Phys. Rev. B **59**, 1758 (1999).
[33] G. Kresse and J. Furthmller, Phys. Rev B **54**, 11169 (1996).

DOI:10.1063/1674-0068/cjcp2108145